PCCP

RSC Publishing

PERSPECTIVE

View Article Online
View Journal | View Issue

Charge trapping in TiO_2 polymorphs as seen by Electron Paramagnetic Resonance spectroscopy

Cite this: *Phys. Chem. Chem. Phys.*, 2013, **15**, 9435

Mario Chiesa, Maria Cristina Paganini, Stefano Livraghi and Elio Giamello*

Received 13th February 2013,
Accepted 23rd April 2013

DOI: 10.1039/c3cp50658d

www.rsc.org/pccp

Electron Paramagnetic Resonance (EPR) techniques have been employed to investigate charge carrier trapping in the two main TiO_2 polymorphs, anatase and rutile, with particular attention to the features of electron trapping sites (formally Ti^{3+} ions). The classic CW-EPR technique in this case provides signals based on the *g* tensor only. Nevertheless a systematic analysis of the signals obtained in the various cases (anatase and rutile, surface and bulk centers, regular and defective sites) has been performed providing useful guidelines on a field affected by some confusion. The problem of the localization of the electron spin density has been tackled by means of Pulse-EPR hyperfine techniques on samples appositely enriched with ^{17}O. This approach has led to evidence of a substantial difference, in terms of wavefunction localization between anatase (electrons trapped in regular lattice sites exhibiting delocalized electron density) and rutile (interstitial sites showing localized electron density).

1. Introduction

Titanium dioxide (or titania) is a solid material with a Janus-faced character, showing two distinct and somehow opposite faces. The first one is that of a material useful for several large scale practical applications. More than four million tons of TiO_2 are prepared per year, to be used, as a white and opaque pigment, in conventional applications such as paintings, food additives, cosmetics, toothpastes, drugs, paper and plastics. The second face of titanium dioxide is that of a sophisticated functional material attractive for advanced applications among which photochemistry is probably the most prominent. Since the fundamental discovery of water photosplitting under UV irradiation in 1972,[1] titanium dioxide has been considered an efficient photocatalyst[2,3] and has been used in reactions for mineralization of water and air pollutants.[4] Later, titanium dioxide has been employed in photochemical processes as a bactericide[5,6] in photokilling of tumor cells,[5] in odour control,[7] and as a superhydrophilic antifogging agent.[8] Additionally, in recent years, the use of titanium dioxide in solar energy conversion processes based on dye sensitization of the solid has become very important.[9] The photocatalytic applications listed above (except for the dye sensitisation which follows a particular route) have a common starting point. Irradiation of a crystal of the oxide entails the initial excitation event followed by charge spatial separation. This leads to the promotion of an electron (e^-) in the conduction band (CB) and the formation of an electron hole (or hole, h^+) in the valence band (VB). The initial light induced separation is followed by charge migration to the surface, charge trapping and, eventually, charge transfer to adsorbed entities.[10,11] All the above steps are the object of often sophisticated investigations and are still not yet fully understood. In particular the nature of the charge traps, their location (surface, subsurface, bulk), the stability of the trapped charge and their propensity to detrapping are all issues of vital importance.

The surface of the solid is deeply involved in its photoactivity and it is therefore not surprising that titanium dioxide has been widely investigated from the point of view of the surface science as reviewed in some extensive review papers.[12–14] Very intense is, in parallel, the computational activity aimed to explore the structure of the surface[15,16] and the phenomena of charge transport[17] and stabilisation.[18]

Trapped electrons and trapped holes can form in TiO_2 also because of chemical modifications of the solid. Titanium dioxide in fact belongs to the class of reducible oxides as it easily loses oxygen upon annealing under vacuum with formation of oxygen vacancies ($V_O^{\bullet\bullet}$ is an empty vacancy in the Kröger–Vink notation) and, in parallel, of excess electrons.

$$O^{2-} + 2Ti^{4+} \rightarrow \frac{1}{2}O_2 + V_O^{\bullet\bullet} + 2Ti^{4+} + 2e^- \rightarrow \frac{1}{2}O_2 + V_O^{\bullet\bullet} + 2Ti^{3+} \quad (1)$$

By losing oxygen the insulating oxide becomes an n-type semiconductor. Excess electrons generated by the oxygen depletion are stabilized into the reduced solid and deeply influence its

Dipartimento di Chimica and NIS, Università di Torino, Via P. Giuria 7, 10125 Torino, Italy. E-mail: elio.giamello@unito.it

chemical and physical properties including catalytic and photocatalytic ones. Although, as pointed out by M. H. Henderson in a recent review paper,[14] some caution must be taken when comparing excess electrons (or holes) formed because of an alteration of the oxide stoichiometry with those due to photoexcitation, the study and the classification of trapping sites in the various TiO_2 polymorphs are undoubtedly very useful. The principal and most investigated polymorphs of titanium dioxide are rutile (R, the thermodynamically stable phase) and anatase (A) while less explored are the properties of brookite (B). All three polymorphs are built up by distorted octahedral TiO_6 units connected by corner and edge sharing and differing in the arrangement of the various interconnections. All oxygen are surrounded by three Ti ions (OTi_3). The two main polymorphs have similar band gap energy (3.0 eV and 3.2 eV for R and A respectively) and differ in terms of the more stable crystal faces which are (110) in the case of rutile and (101) in the case of anatase. The relatively small difference between anatase and rutile causes however important distinctions in their behaviour. In particular anatase is more active in photocatalytic terms than rutile even though the maximum photocatalytic activity is usually observed in the case of P25, a mixed phase system produced by Degussa, whose peculiar properties have been recently discussed in terms of an active interface between A and R phases which would favour the spatial separation of the photo-generated charges.[19] Since rutile is the most thermodynamically stable polymorph and its single crystals are easily available, this phase has long been the most investigated one by surface science while anatase, due to its better photocatalytic performances, has been more considered in applied photocatalysis studies and, consequently, in characterisation activities using polycrystalline solids. This has caused therefore a certain imbalance in the literature in particular for the relatively poor number of single crystal studies on anatase.

When excess electrons are generated in titania they are usually stabilized by metal cations with formation of Ti^{3+} units (second part of eqn (1)). In spite of the fact that, in some cases, the presence of electrons trapped in oxygen vacancies has been invoked (mainly on the basis of optical absorption[20]) unambiguous evidence for the presence of such centres (color centres or F centres) in titanium dioxide has, in our opinion, never been provided. Moreover modern and accurate theoretical calculations firmly indicate that electrons released in the solid by oxygen depletion are preferentially stabilized on Ti d orbitals.[21]

Actually the presence of Ti^{3+} in reduced or in irradiated TiO_2 is well documented by EELS,[22] polarized optical spectroscopy,[23] photoelectron spectroscopy[24] and, in particular by Electron Paramagnetic Resonance (EPR)[25]spectroscopy which is the main technique adopted by our group to investigate bulk and surface defects in solids and radical intermediates at solid surfaces.[26,27] EPR techniques are, beyond any doubt, the reference techniques for detection of radicals and, in general, of paramagnetic species. The advantages of EPR, beside its specificity, are more than one. In particular EPR is highly sensitive, it provides information on the symmetry of the paramagnetic centre and, in the case of presence of nuclei having non-zero nuclear spin interacting with the unpaired electron, it allows detailed mapping of the electron spin density *via* the so called hyperfine interaction. A further advantage, particularly useful in the studies of oxides photochemistry, is the low frequency of the electromagnetic radiation needed for electron spin resonance (in the range of microwaves) which allows recording EPR spectra either in the dark or under irradiation with higher frequency light (UV, visible, infrared) without interference, thus increasing the number of experimental opportunities. The EPR technique has been used, on the one hand, in studies of excess electrons in rutile single crystals[25c,f,28–30] mainly aiming to understand the symmetry of Ti^{3+} centres. On the other hand investigations on polycrystalline TiO_2 systems can be divided into two types *i.e.* those mainly devoted to phenomenological aspects of the oxide behaviour and of its surface chemistry (formation of reduced Ti^{3+} centres under various conditions, reactivity towards adsorbates, *etc.*) and those aiming to elucidate the effect of the solid irradiation in terms of charge trapping and surface charge transfer.[19,31] In spite of this considerable experimental effort, however, several questions concerning the nature and location (surface or bulk, lattice or interstitial) of the centres detected by EPR for the various polymorphs remain open. In particular a conclusive assignment of each EPR signal observed in TiO_2 to a well-defined centre is still incomplete. Additionally, a fundamental question which remains open and is the focus of a lively debate is related to the nature of the electronic states associated with excess electrons in titania whose wave function has been already described either as localized on a single titanium ion or delocalized over several of them. This problem has been tackled by several groups using sophisticated experimental approaches such as resonant photoelectron diffraction[32] or STM[33] and by a number of theoretical investigations. EPR, until a short time ago, did not contribute to this debate because of the absence of hyperfine structure in the spectra of both trapped electrons and trapped holes. As it will be clarified in the following sections the first EPR data on hyperfine interactions in TiO_2 now appear in the literature thanks to the techniques of enrichment of the solid with suitable isotopes (*vide infra*).

The present paper is devoted to a survey of EPR results from our laboratory on trapped charge carriers (mainly excess electrons) in TiO_2 with the aim of rationalizing the somehow blurred picture today available with convincing assignments. In particular we aim to distinguish the behaviour of the two main polymorphs and to illustrate the various ways to generate trapped electrons and holes in the solid. For the sake of simplicity we refrain from discussing in this paper the results obtained on non-metal-doped titanias, in particular N–TiO_2 and related systems, using a similar approach.[34] Doped titanias are studied mainly to obtain solids showing photoactivity under visible light. The bulk of concepts and results recently produced in this particular field are large enough to deserve a specific discussion.

2. Materials and methods

The studies accounted in the present paper were performed on TiO_2 prepared *via* various distinct procedures. In the case of anatase we have carried out two types of sol–gel preparations *via* hydrolysis of titanium(IV) isopropoxide and of $TiCl_4$ respectively.

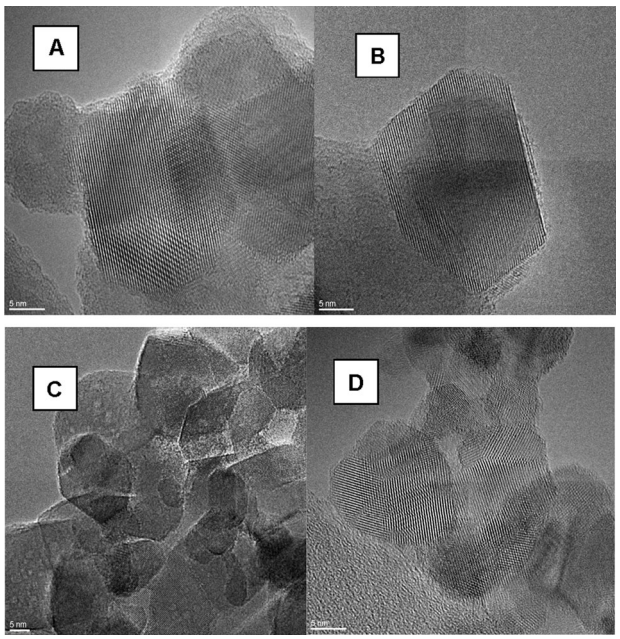

Fig. 1 TEM images of four differently prepared anatase materials. (A) Prepared by sol gel of Ti isopropoxide and successive calcination at 773 K for 1 hour. (B) Prepared by sol gel of Ti isopropoxide and successive calcination at 773 K for 24 hours. (C) Prepared by hydrolysis of $TiCl_4$ and successive calcination for 1 h. (D) Prepared by Chemical Vapor Reaction (CVR).

Details of these preparations have been reported elsewhere. The dried material after hydrolysis was heated at 773 K in air at different time intervals. Another type of anatase was prepared by Chemical Vapour Reaction by oxidation of titanium isopropoxide vapours in a home made flow reactor. The resulting powders were characterized by X-ray diffraction, surface area measurements and Transmission Electron Microscopy. Fig. 1 reports TEM pictures of the four anatase samples considered in the present investigation. The morphological features of the same samples are reported in Table 1.

All experiments aimed to monitor the features of electron or hole trapping centres gave similar results for all the samples, the only difference being, in some cases, a variation of the relative intensities of the EPR peaks of the various species. In quantitative terms the whole intensity of the signals showed moderate variations from case to case related to the crystal size.

Experiments on rutile were performed either on commercial powders from Aldrich (microrutile and nanorutile respectively) or on solids obtained by high temperature treatment of the anatase systems described before. Reduced (blue) rutile TiO_2 was prepared by hydrolysis of $TiCl_4$ with a stoichiometric amount of water under N_2 flow. The powder was kept under N_2 flow for 2 hours and successively transferred in a quartz tube and heated up to 973 K for 10 minutes under N_2 flow. ^{17}O enrichment of TiO_2 samples (anatase or rutile) was obtained by employing ^{17}O isotopically enriched water (40% ^{17}O enrichment supplied by Icon Services, New Jersey).

Table 1 Morphological features of the four anatase samples reported in Fig. 1

Sample label (Fig. 1)	Crystallographic phase	Average crystal size/nm (Rietveld refinement)	Specific surface area/$m^2\ g^{-1}$ (B.E.T. method)
A	Anatase	21	47
B	Anatase	43	26
C	Anatase	24	46
D	Anatase	6	150

3. Electron Paramagnetic Resonance and titanium dioxide: the *g* tensor of trapped electrons and holes

Conventional CW-EPR (Continuous Wave-EPR) has been until now largely dominant in titanium dioxide studies. In a CW-EPR experiment the substance under investigation interacts with a homogeneous magnetic field which is allowed to vary in a selected range and is irradiated by a continuous flow of microwaves at fixed frequency which, when resonance conditions are fulfilled, entails a transition between two spin states. Microwaves belonging to the X-band (about 9.5 GHz) are the most commonly used even though in some case higher frequencies are useful to resolve particular spectra. A CW-EPR spectrum reports the first derivative of the microwave absorption as a function of the swept magnetic field measured in Tesla or in Gauss (1 Tesla = 1×10^4 Gauss). Pulse EPR (a method based on irradiation by short microwave pulses) was introduced more recently. However pulsed techniques started to undergo rapid development and are now finding a wider range of applications. For details of the principles of EPR techniques and applications to solid state and catalysis studies the reader is referred to recently published books or specialist reports.[35,36] Ti^{3+} is paramagnetic ($S = 1/2$) having a $3d^1$ configuration. In solid crystals the ground state of the free ion is split by the effect of a crystal field. Since in all TiO_2 polymorphs the dominating symmetry is octahedral, we will limit our discussion exclusively to this case. When the metal ion is octahedrally coordinated, the free-ion ground state is split so as to give two subgroups with three t_{2g} and two e_g orbitals separated by the energy term Δ_O. An additional tetragonal (Scheme 1A) or trigonal (Scheme 1B) distortion further lifts the degeneracy of the t_{2g} and e_g levels and results in anisotropic *g* values. In the tetragonal case (D_{4h}), if the distortion is a tetragonal compression, the ground state is the d_{xy} orbital (Scheme 1A(a)), while if the distortion is a tetragonal elongation (Scheme 1A(b)), the ground state is a degenerate d_{xy}, d_{yz} orbital. In the latter case, Ti^{3+} exhibits a Jahn–Teller effect that further resolves the degeneration. The *g* value expressions for a Ti^{3+} ion in a tetragonally distorted octahedral environment are:

$$g_{\parallel} \cong g_e - (8\lambda/\delta_2) \text{ and } g_{\perp} \cong g_e - (2\lambda/\delta_1) \qquad (2)$$

where δ_1 and δ_2 are the energy separation between the d-orbitals shown in Scheme 1A. In the case of trigonally distorted octahedral (D_{3d}) symmetry the five orbitals are split into three energy states, as shown in Scheme 1B. We include this case for the sake of completeness, however trigonal distortions do not occur in TiO_2.

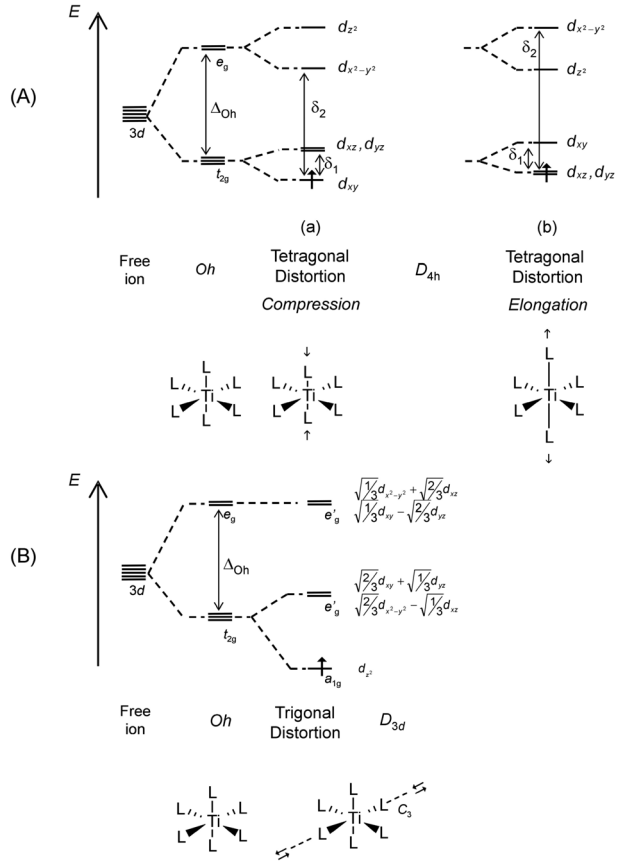

Scheme 1 Level scheme for the d-orbitals of Ti^{3+} undergoing (A) tetragonally and (B) trigonally distorted octahedral crystal field.

The resulting d orbitals are quantized with respect to the three-fold axis, and the unpaired electron dwells in the d_{z^2} orbital. The theoretical g values are:

$$g_{\parallel} = g_e \text{ and } g_{\perp} = g_e - (2\lambda/\delta) \quad (3)$$

Although CW-EPR can provide evidence for the local symmetry adopted by Ti^{3+} ions, the details of the metal to ligand interaction and the coordination geometry of first and second shells remain largely undetermined. Insights into this direction can be obtained using advanced EPR methods when isotopic enrichment in magnetically active isotopes is obtained. The main isotopes of Ti and O are ^{48}Ti and ^{16}O both having nuclear spin $I = 0$. The abundance of Ti magnetic isotopes *i.e.* ^{47}Ti ($I = 5/2$ natural abundance 7.44%) and ^{49}Ti ($I = 7/2$ natural abundance 5.41%) is, in most cases of solid systems, not high enough to produce a detectable hyperfine structure. The same applies for ^{17}O ($I = 5/2$) whose natural abundance is only 0.037%. The information provided by the hyperfine structure, essential to monitor the localisation degree of the wavefunction, is therefore absent in the spectra of electrons and holes trapped in TiO_2 when the constituent elements are in natural abundance.

An electron hole at the surface of a metal oxide or in correspondence of a cation vacancy (in the second case the defect is known as a V centre) localizes on oxide anions producing a paramagnetic centre which, in chemical terms,

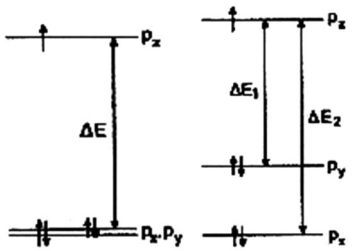

Scheme 2 Energy levels of O^- ions in axial and rhombic symmetry.

can be described as an O^- ion ($O^{2-} + h^+ \rightarrow O^-$) having the unpaired electron hosted in a 2p orbital. This fact is confirmed by both theoretical and experimental EPR results.[37] According to the symmetry of the environment the g tensor can be either axial or rhombic (Scheme 2).

The expected g values in the axial case are:

$$g_{\parallel} = g_{zz} \approx g_e; \quad g_{\perp} = g_e + 2\lambda/\Delta E \quad (4)$$

In rhombic symmetry one has:

$$g_{zz} \approx g_e; \quad g_{xx} = g_e + 2\lambda/\Delta E_1; \quad g_{yy} = g_e + 2\lambda/\Delta E_2 \quad (5)$$

4. Charge trapping centres in TiO_2: EPR results

As discussed in Section 1 charge carriers are trapped in the oxide matrix as a consequence of photochemical charge separation or, alternatively, of chemical treatments modifying the solid (*e.g.* annealing under vacuum, chemical reduction). A systematic knowledge of the features of trapped electrons and holes is of vital importance to rationalize the behavior of the various polymorphs. We report here a systematic analysis of the EPR results obtained for trapped electrons and holes in TiO_2 polymorphs (essentially A and R). This is done in order to classify the diverse types of EPR signals (g values, lineshape, *etc.*) and, possibly, to establish a correspondence between the signals themselves and the variety of trapping sites.

4.1 Valence induction

The method is well known in solid state chemistry and consists of the introduction, in regular positions of the solid network, of elements having extra electrons or an electron deficiency with respect to Ti and O. Excess electron solids can be obtained both by cationic and anionic substitution. In the first case Nb or Sb ions have been used to substitute Ti while, in the second case, fluorine substitutes lattice oxygen. Alternatively, electron deficient systems can be obtained by introducing Al in the crystals. In the case of polycrystalline TiO_2 the substitution is easily achieved using wet chemistry preparations of the solid such as the sol–gel technique or hydrothermal methods which easily lead to doped anatase. In the case of anatase the excess electrons are trapped under the form of Ti^{3+} centres which are visible in the EPR spectra. The two types of excess-electron solids (cation or anion substitution) can be written, respectively, as $Ti_{(1-x)}^{4+}$

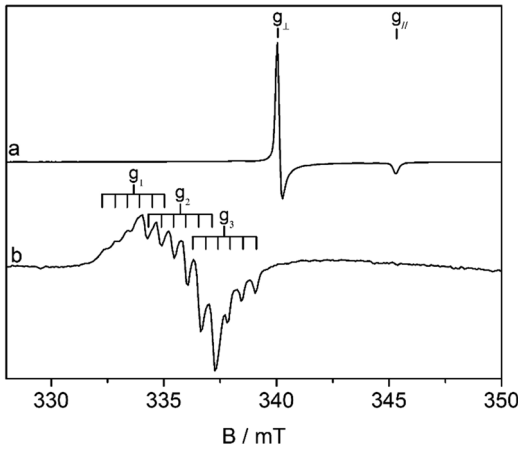

Fig. 2 EPR spectra of a trapping electron centre (a) and a trapping hole ($Al–O^-$) centre in anatase (b). In the latter case the intensity of the original signal has been enhanced by a short irradiation.

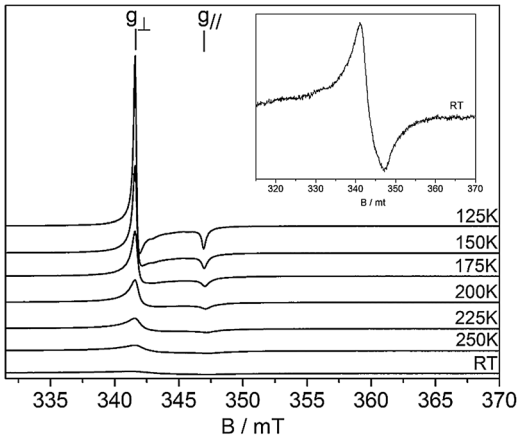

Fig. 3 EPR spectra of Nb doped anatase in the temperature range 125 K–RT. In the inset the spectrum at RT is reported with higher magnification.

$Nb_x^{5+}\ Ti_x^{3+}\ O_2^{2-}$ and $Ti_{(1-x)}^{4+}\ Ti_x^{3+}\ O_{(2-x)}^{2-}\ F_x^-$. Niobium doping of polycrystalline anatase has been previously investigated by EPR by Kiwi *et al.*[38] and by Valigi *et al.*,[39] while fluorine doping was reported by Halliburton (single crystals)[40] and by some of us.[41] In the case of Al doping the solid compensates the effect of the trivalent dopant both creating oxygen vacancies and, though at a minor extent, localizing holes onto oxygen ions (O^- h^+). Fig. 2 shows the X band EPR spectra, recorded at 77 K, of a Nb doped material (2a) and of an Al doped (2b) material. The former spectrum is similar to those obtained using Sb or F.

The Ti^{3+} signal in Fig. 2a (hereafter signal A) is axial (g_{zz} = $g_{\parallel}$ = 1.962 and g_{xx} = g_{yy} = $g_{\perp}$ = 1.992) and no break of this symmetry is observed even when the spectrum is recorded at much higher resolution (W band, 95 GHz).[42] As illustrated before this spectrum is the result of the compensation of the extracharge carried by the dopant. Recording the spectrum at increasing temperatures (Fig. 3) the line tends to broaden, the intensity to decline and eventually to disappear. There are two possible causes of the described effect which are probably both operating in this case. The first one is the trend of the relaxation time values which, in several cases of Ti^{3+} spectra, causes weakening of the intensity at temperatures higher than that of liquid nitrogen (77 K). The second one is thermalisation of electrons from intra band gap states to the conduction band. To observe this effect at around room temperature the intra-band states must be, of course, very shallow (see Section 4). The paramagnetic centre corresponding to signal A constitutes the prototype of an electron-trapping site in bulk regular positions of the anatase lattice (thus not associated with oxygen vacancies). The same conclusion was reached by studies on photoinduced charge separation in irradiated TiO_2 systems kept in aqueous colloidal suspensions.[31,43,44]

Experiments in rutile with the same approach are not easily feasible. In fact if F-doped anatase is heated at high temperature to accomplish the anatase to rutile phase transition the sample loses completely the fluorine dopant. In the case of Nb doped titania it has been instead clear, since the early studies of Chester[45] and Zimmermann[46] on single crystals, that the excess electron resides on the dopant metal. In these papers the authors observe at very low temperature the EPR spectrum of Nb^{4+} ions with the typical hyperfine structure of ^{93}Nb (I = 9/2). In our powdered material the transformation of Nb doped anatase in rutile by high temperature treatment causes the modification of the EPR signal which moves at a higher magnetic field at g = 1.981 (as expected in the case of Nb^{4+}) but the rich hyperfine structure remains unresolved at 77 K (data not reported for brevity). To summarize, the valence induction in TiO_2 using excess electron elements surprisingly leads to different results in the case of anatase and rutile. In the former case (F, Nb, Sb doping) the electron trapping sites are lattice titanium ions (and the axial signal A is the EPR fingerprint of such sites) while in the second case (Nb doped rutile) the electrons remain on the aliovalent dopant element.

The spectrum in Fig. 2b has been obtained in the case of Al^{3+} doped TiO_2 and is clearly due to an electron hole localized onto an O^{2-} ion proximity of an Al ion. The spectrum is rich of lines because of the hyperfine interaction with the I = 5/2 ^{27}Al nucleus. The g values of the rhombic signal are g_1 = 2.027, g_2 2.015, g_3 = 2.003 and are typical of an O^- ion, which is the chemical manner to describe an electron hole localized on an oxide ion: (O^- h^+). The hyperfine tensor of ^{27}Al is A_1 = 0.5 mT, A_2 = 0.58 mT, A_3 = 0.61 mT. The g values of the AlO^- hole centre are close to those of similar centres in other solids (SiO_2,[47] ZrO_2[48]). The reason for the hole localization close to an Al^{3+} ion has to be searched in the small size of this cation which exerts a strong electrostatic potential on the O^- ion.

4.2 Photoexcitation

The effects of UV irradiation of TiO_2 have been already described in several papers mainly concerning anatase and P25. The seminal work in the field was performed by Graetzel and Howe[31] on anatase and by the Thurnauer group mainly on the biphasic P25 system.[43] In both cases the authors irradiated at very low temperature colloidal aqueous suspensions (systems used in photocatalytic tests at RT). The presence of surface

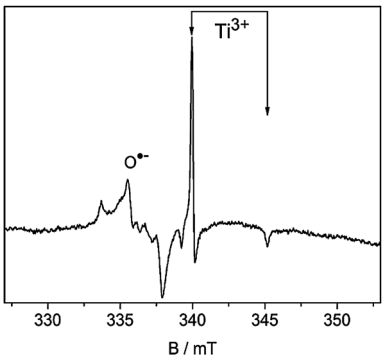

Fig. 4 EPR spectra recorded at 77 K of CVR anatase under UV irradiation. The spectrum recorded at 1 mW microwave power. The sample is irradiated under vacuum. Rising the temperature at RT the two carriers easily recombine.

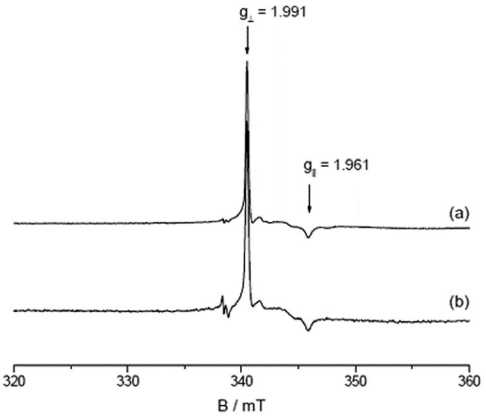

Fig. 5 EPR spectra of CVR anatase contacted with atomic hydrogen (a) and deuterium. (b) They are dominated by the previously discussed signal A which is however perturbed by the onset of a second broad signal. This second signal is better detected by the Electron Spin Echo (ESE) detected EPR experiments (Fig. 6).

hydroxyls and water molecules favors in these cases the stabilization of the carriers.

Although in our experiments we also use polycrystalline materials, our approach is closer to that of surface science and of gas–solid interaction studies. We have thus irradiated fully dehydrated samples kept under vacuum obtaining anyhow evidence of charge separation and trapping (Fig. 4).

Electrons, under these conditions, are also trapped on lattice titanium ions. The signal in Fig. 4, in fact, is the same observed by valence induction (signal A with $g_{\|} = 1.962$ and $g_{\perp} = 1.992$). The trapped hole signal (O^-) is made up by the contribution of at least two akin species with similar but distinct parameters. At the microwave power employed to record the spectrum in Fig. 4 one of these species is dominant and has $g_1 = 2.027$, $g_2 = 2.015$, $g_3 = 2.003$. These values are similar but not exactly coincident with those previously reported[25d] probably due to the fact that the spectrum in Fig. 4 is recorded under vacuum. The holes are trapped at the surface since they easily react with hole scavengers like molecular hydrogen.

4.3 Electron injection

Electron injection in the solid through the surface can be easily achieved by exposing a sample to atomic hydrogen. This can be generated either by microwave discharge in H_2 with direct formation of H atoms over the solid or by UV irradiation in a H_2 atmosphere. In the first case the H atom ionizes injecting an electron in the solid:[49,50]

$$O_{surf}^{2-} + H \rightarrow OH_{surf}^{-} + e^- \quad (6)$$

In the second case the UV light induces charge separation with formation of an electron and a hole. The surface migrated hole reacts with molecular hydrogen to give an hydroxyl group and an H atom:

$$2O_{surf}^{2-} + h^+ + H_2 \rightarrow OH_{surf}^{-} + O_{surf}^{2-} + H \rightarrow 2OH_{surf}^{-} + e^- \quad (7)$$

In both experiments the reducing agent is atomic hydrogen and the results, in terms of EPR spectra, are identical. Fig. 5 reports two EPR spectra, in a restricted magnetic field range, related to a hydrogen treated and a deuterium treated anatase respectively. The two spectra are practically superimposable indicating that there is no appreciable interaction of the unpaired electron with the parent H (D) nucleus.

The ESE detected EPR spectrum (Fig. 6) corresponds to the absorption of the conventional CW-EPR spectrum and is more effective in the detection when, as in the present case, broad signals are present which are hardly observed in the CW derivative spectrum. The spectra of H treated TiO_2 (Fig. 5 and 6) are thus more complex than those in Fig. 2a and 3 as they include two distinct signals. The broad unstructured signal (signal B) is centered at approximately $g = 1.93$ and extends over approximately 35 mT. This means that, despite what appears in Fig. 5, the number of paramagnetic centres corresponding to signal B is much higher than that corresponding to signal A.

The most likely source of broadening, determining the large linewidth of signal B, has been ascribed[42] to strain effects associated with the presence of different sites with slightly different local environment and therefore slightly different

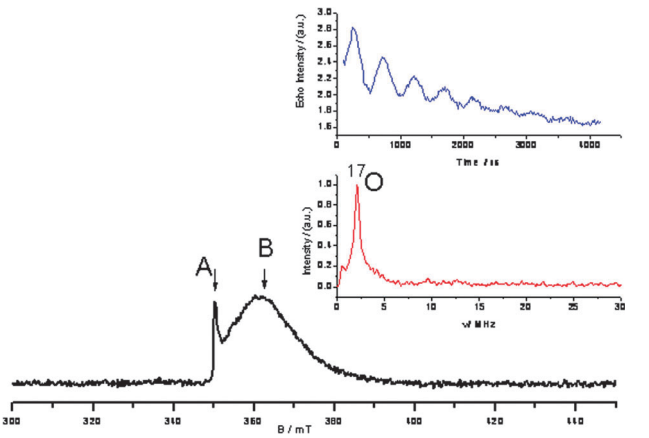

Fig. 6 ESE detected (T = 10 K) EPR spectrum of ^{17}O enriched anatase treated with atomic H. In the inset the 3 pulse ESEEM spectrum taken at observer position B and the corresponding frequency domain spectrum.

EPR parameters. This situation indeed occurs at the surface of anatase nanocrystals which is made up of different faces each of them exposing ions having at least two different coordinations. The presence of morphological defects of the crystals like edges, steps or kinks further complicates the picture. The surface nature of Ti^{3+} ions corresponding to signal B has been confirmed by *ad hoc* ESEEM (Electron Spin Echo Envelope Modulation) experiments on anatase nanocrystals enriched at the surface with ^{17}O.

The local enrichment has been obtained by annealing at 773 K the solid (oxygen depletion) and then restoring the oxygen content by reoxidation in $^{17}O_2$. In this way the surface region, more affected by oxygen depletion, becomes isotopically enriched. The three-pulse ESEEM pattern[42] shows an ^{17}O modulation depth which is rather strong in the case of species B (inset of Fig. 6), indicating a high number of ^{17}O nuclei interacting with the Ti^{3+} centres, and nearly absent in the case of species A (not reported). This can only be explained, as the ^{17}O enrichment is limited to the surface and subsurface region of the sample, in terms of the surface nature of the species corresponding to signal B. The same conclusion on the nature of the broad signal at $g = 1.93$ was proposed by Thurnauer and co-workers[43,51] on the basis of its behaviour upon reactivity of the solid. Summarizing, the electron injection from an external source (H) leads to two types of electron trapping. A minority of the trapped electrons stabilize on the subsurface or bulk Ti^{4+} electron traps (signal A) while the majority (B) are stabilized onto variously coordinated trapping electron ions at the solid surface.

4.4 Reductive annealing of the solid

The propensity of TiO_2 to lose oxygen by annealing under vacuum transforming from an insulator to an n-type semiconducting oxide has been described in the introduction (eqn (1)). Oxygen depletion generates, besides oxygen vacancies, excess electrons which are trapped in the solid. Fig. 7 describes in terms of EPR the effect of a progressive reduction of anatase by sequential annealing steps (15 min each) from 470 K to 770 K.

The figure shows that, in the early stages of the reduction, the bulk Ti^{3+} species (species A, narrow signal) is clearly visible in the spectrum and its intensity grows till the annealing step at 573 K. In the following steps of the treatment the signal of species A tends to overlap with the broad and featureless line of signal B, the surface titanium reduced species at $g = 1.93$ already described in Section 4.3. Eventually signal B becomes dominant in the EPR spectrum and the disordered, defect-rich phase corresponding to this signal expands to encompass the subsurface region where species A was initially present. Under such conditions the anatase sample is colored (pale grey-blue) and EPR spectra recording becomes difficult due to the presence of conduction electrons in the material.

4.5 Electron trapping centres in rutile

In the case of rutile the surface treatment described in Sections 4.3 and 4.4 leads to signals which often tend to become broad and featureless particularly in the case of extremely small crystals. This has caused some confusion in the literature. To determine exactly the typical parameters of excess electrons in rutile it is necessary to explore the early stages of electron injection as done in the experiments reported in Fig. 8 where two EPR spectra obtained by gentle annealing of microcrystalline rutile (Fig. 8a and b) are compared. Strictly similar spectra are obtained by reaction with H atoms. Both spectra in Fig. 8 are due to Ti^{3+} centers. The first one (8a) shows up after a short annealing at 373 K while the second (8b) appears after a similar treatment at 673 K. The two signals are basically the same except for the linewidth which is larger in the second spectrum, as shown by computer simulation. The signal in Fig. 8a due to its low intensity is fully resolved and has an orthorhombic g tensor with $g_1 = 1.969$, $g_2 = 1.960$ and $g_3 = 1.949$. It is absolutely reasonable to consider these parameters as prototypes for the regular lattice titanium site (hereafter C) trapping an electron

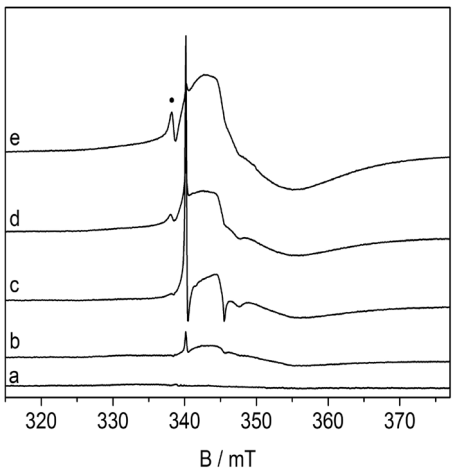

Fig. 7 Thermal annealing under dynamic vacuum of sol–gel prepared anatase at increasing temperature adopting 15′ steps. (a) Starting material, (b) 470 K, (c) 570 K, (d) 670 K and (e) 770 K.

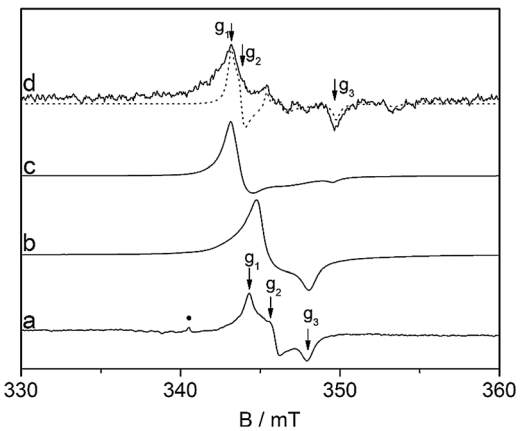

Fig. 8 EPR spectra recorded at 77 K of microrutile annealed under vacuum at 373 K (a) and at 673 for 15 min (b). The dot in (a) indicates a trace of Ti^{3+} ions in anatase (signal A). EPR spectra at 4 K of the as prepared ''blue'' rutile sample prepared *via* hydrolysis of $TiCl_4$ and observed by CW-EPR (c) and ESE-detected EPR (d).

Table 2 *g* values of various electron trapping centers in anatase and rutile

Signal	Polymorph	Trapping site	*g* Values			Notes
A	Anatase	Regular lattice site (bulk)	$g_{\perp}$ = 1.992	$g_{\parallel}$ = 1.962		Narrow (Fig. 1). Formed by: (i) valence induction, (ii) photoexcitation, (iii) electron injection and (iv) reductive annealing
B		Surface sites (disordered environment)	g_{av} = 1.93			Broad because of site heterogeneity (Fig. 4). Formed by (i) electron injection and (ii) reductive annealing
C	Rutile	Regular lattice site	1.969	1.960	1.949	Formed by: (i) electron injection and (ii) gentle reductive annealing
D		Interstitial site	1.9787	1.9750	1.9424	Formed by: (i) substoichiometric preparation and (ii) extreme reductive conditions[52]

(Ti^{3+}). Differently from the case of anatase (Fig. 6 and 7) no signal at different *g* arises for prolonged annealing, the only result being a progressive broadening of the original signal which eventually becomes featureless. There is not, therefore, a clear evidence of the presence of two distinct signals for bulk and surface electron traps.

The question of the presence in reduced rutile (and in general in titanium dioxide) of significant amounts of ions located in interstitial sites has been widely discussed in the literature in particular when considering ion migration during reoxidation of surfaces reduced by sputtering[52] which occurs *via* diffusion of bulk cations occurring also through interstitial positions. Apart from this evidence which concerns a dynamic phenomenon, evidence of the presence of stable interstitial Ti^{3+} centres in reduced rutile was obtained by EPR for a series of single crystals[53] and in the case of a single crystal rod, studied by Aono and Hasiguti, heated in a preevacuated capsule in the range 1300–1700 K.[54] In the second case only, the authors were able to derive the exact orientation of the observed Ti^{3+} species in the crystal (firmly proving the interstitial nature of the center) and provided the principal elements of its *g* tensor (g_1 = 1.9780, g_2 = 1.9746 and g_3 = 1.9414).[54] In the case of polycrystalline materials and differently from anatase, the rutile polymorph can be directly prepared in sub-stoichiometric form. Blue colored TiO_2 materials are quite highly reduced but are stable in air. Due to their visible light absorption properties, such materials have been seldom used in experiments of photocatalysis under visible light.[55] We have directly prepared reduced rutile by hydrolysis of $TiCl_4$ with a stoichiometric amount of water under N_2 flow. The powder was kept under N_2 flow for 2 hours and successively heated up to 973 K for 10 minutes under N_2 flow. The final product was a blue TiO_2 powder mostly in the rutile form. The sample shows an EPR signal at 4 K which is reported in Fig. 8c and d. In the second case the spectrum is the first derivative of an Electron Spin Echo (ESE) detected spectrum which is well resolved and allows an accurate measure (see computer simulation) of the *g* tensor elements which are[56] g_1 = 1.9787, g_2 = 1.9750 and g_3 = 1.9424, compatible with a tetragonally distorted octahedral symmetry of the centre further reduced by an intrinsic local asymmetry of the Ti coordination (*vide infra*).

This set of parameters of the rhombic signal observed in polycrystalline blue rutile (Fig. 8c and d) nearly exactly coincide with those recorded in the mentioned single crystal study.[54] On the basis of the close similarity of the two sets of parameters, the signals in Fig. 8c and d (signal D) must be considered the powder EPR spectrum of interstitial Ti^{3+} ions in rutile. The distinction between regular lattice sites and interstitial sites in rutile is very small as the *g* values of the signals (Fig. 8) are quite close to each other but unambiguously distinct. This is not very surprising if one considers the coordination of titanium ions in the two sites (lattice and interstitial) which are extremely similar. A scrutiny of the rutile structure[57] indicates, in fact, that the coordination of titanium ions in the lattice position and in the interstitial position of this structure mainly differs in the orientation of the fourfold axis since in both cases one has an octahedrally distorted environment of oxygen spheres. This is not the case of anatase where an interstitial site has a quasi-pyramidal symmetry lower than that of the regular site.[58]

The *g* values of the main electron trapping sites present in the two main polymorphs of TiO_2 are resumed in Table 2 together with the conditions of their formation.

The asymmetry observed in Table 2 and related to the lack of signals due to interstitial Ti^{3+} in anatase, has been partially commented before. We can add here that the presence of interstitial Ti^{3+} in anatase (which is unlikely due to the strong asymmetry of the site discussed just above) cannot be however completely excluded. The signals of these sites (if any) may be buried in the broad signal B whose width implies a strong heterogeneity. It is more difficult to comment on the absence of distinct signals for surface and bulk Ti^{3+} in rutile. This could be due to a possible lower stability of one of these species with respect to the other with consequent migration of the excess electrons from the surface towards the inner sites of the solid or viceversa. Work is in progress in our laboratory for a conclusive clarification of this issue.

5. Electron localization in trapping centres

As mentioned in the introduction the space distribution of the trapped electron wave function is critical for all applications of TiO_2 implying generation, stabilisation and dynamics of charge carriers. This question is still debated and opposite conclusions (electron localized on a single titanium ion or delocalized on several ions in a relatively large volume) are often derived using various experimental approaches.[32,33] Furthermore, the theoretical descriptions of reduced titanium oxide do not contribute to solve the dilemma since, as recently shown, it happens that fully localized and highly delocalized solutions show similar energy values limiting the possibility of a clear indication derived from theory.[21] As far as EPR is concerned, the spin density distribution, which is a strong point of the technique,

cannot be derived in the case of Ti^{3+} ions since the g factor only is available. The absence in the system of magnetic nuclei (nuclear spin $I \neq 0$) in sufficient concentration, in fact, prevents the measurement of the electron–nucleus interaction (hyperfine interaction) which is the parameter providing information on the spin density distribution. To start overcoming this problem and considering that the direct insertion in the solid of Ti magnetic nuclei (^{47}Ti and ^{49}Ti) is not an easy task, our group has proposed a method based on the inclusion by chemical methods of ^{17}O (I = 5/2) into the oxide lattice. This method, successfully adopted in the case of alkali earth oxides[59] which have the same problem of isotopic composition found in TiO_2, allows the measure of the so called superhyperfine interaction. This interaction, in principle, allows us to measure the electron spin density localized onto the ligands of a coordination compound having a paramagnetic metal centre. In our case we intended to evaluate the spin density on the oxygen atoms surrounding Ti^{3+} in TiO_2. To obtain ^{17}O bulk-enriched TiO_2 various preparations of the oxide by hydrolysis of $TiCl_4$ employing ^{17}O enriched water were performed. We thus obtained in this way bare anatase, F-doped anatase and blue reduced rutile (Section 4.5). Fully oxidized rutile was obtained by anatase transformation. The typical CW-EPR spectra of Ti^{3+} in anatase and rutile shown before in this paper do not change after ^{17}O enrichment indicating that the expected superhyperfine interactions are too small to be detected by this technique. Therefore, in order to probe the spatial extent of the unpaired electron wave function for these Ti^{3+} interstitial ions, Hyperfine Sublevel Correlation spectra have been recorded at different field positions corresponding to the principal g values of the dominant EPR signals on two different samples namely F doped anatase (bulk lattice site, Table 2 species A) and substoichiometric rutile (interstitial site; Table 2 species D). Typical HYSCORE spectra are reported in Fig. 9 and show the presence of different ^{17}O correlation peaks in both (+,+) and (−,+) quadrants, which are absent in the non-enriched samples. The most striking difference between the two samples is in the strong hyperfine region (−,+ quadrant, left hand side of the figure). In the case of substoichiometric rutile in fact two off diagonal cross peaks at about (−2.6) MHz and (−6.2) MHz in the (−,+) quadrant are present, which are separated by approximately $2\nu_O$ (ν_O = 2.021 MHz) and relate the ^{17}O $m_I \frac{1}{2} \rightarrow -\frac{1}{2}$ transitions of the two m_S manifolds. Computer simulation analysis of spectra recorded at various magnetic field positions allowed us to extract the full ^{17}O hyperfine tensor.[56] From these values a Fermi contact (a_{iso}) term of about 8 MHz and an anisotropic coupling $2T \approx$ 2 MHz were derived (Table 3). The origin of this (negative) Fermi contact term can be understood considering the nature of the chemical bond between the Ti ions and the oxide ligands. The bonding interaction in TiO_2 is characterized by a π overlap between the metal d and oxygen p orbitals[60] This interaction when paramagnetic Ti^{3+} ions are present will induce, in a negative spin density on the oxygen as a result of a spin polarization mechanism, the positive sign of a_{iso} being due to the negative ^{17}O nuclear g factor (g_n = −0.757516). This fairly large (positive) ^{17}O hyperfine constant appears to be indeed a distinctive feature of d^1 metal–oxygen bonding mechanisms as observed in some

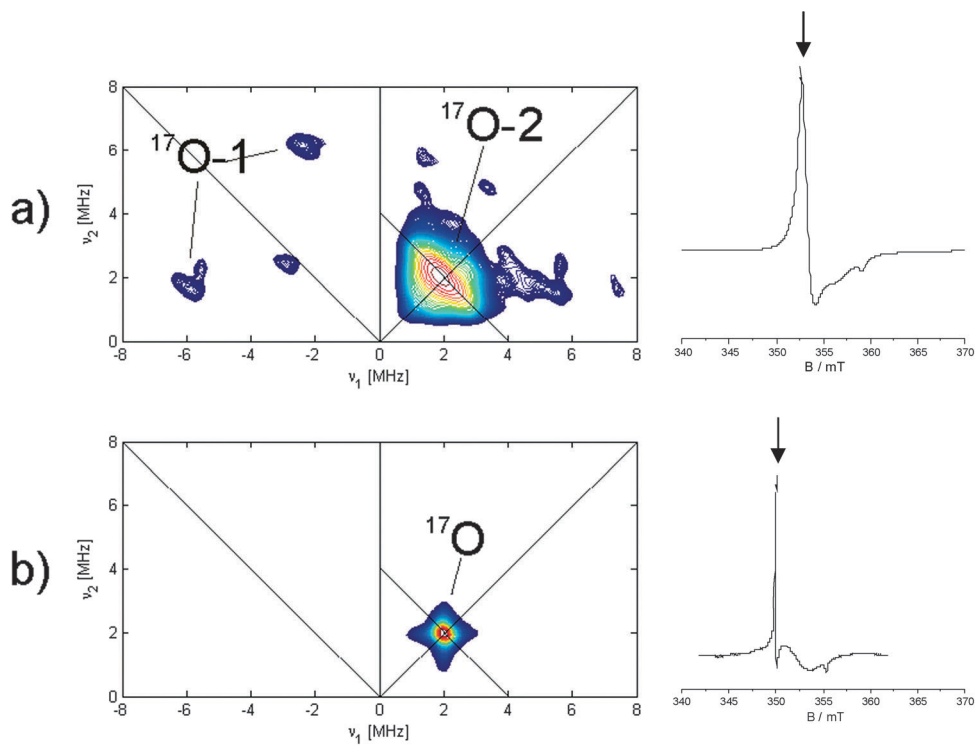

Fig. 9 ^{17}O HYSCORE spectra of (a) interstitial Ti^{3+} ions in rutile and (b) Ti^{3+} ions in F doped anatase. The corresponding CW EPR spectra are shown on the right hand side of the figure. HYSCORE spectra were recorded at 4 K with τ = 120 ns. The observer position corresponds in both cases to the perpendicular component of the EPR spectrum and is indicated by an arrow in the EPR spectra.

Table 3 Comparison of the *g* and ^{17}O hyperfine parameters concerning the Ti^{3+} species discussed in this paper

	g Tensor			^{17}O A tensor/MHz				
System	g_1	g_1	g_1	a_{iso}	A_1	A_2	A_3	Ref.
Esaquo Ti^{3+}	1.994	1.896	1.896	7.5	−0.5	2.0	−1.5	62
Interstitial Ti^{3+} in the rutile single crystal	1.9780	1.9746	1.9414	—	—	—	—	54
Ti^{3+} in ^{17}O rich reduced rutile (sign. D)	1.9787	1.9750	1.9424	8	−2.5	0.5	2.0	56
Ti^{3+} in anatase lattice sites (sign. A)	1.9920	1.9920	1.960	<0.2	und.	und.	und.	42

esaquo molecular cations where metal–oxygen bonds are based on π overlap interactions.[61] Based on the similarities between the nature of the chemical bond between solid TiO_2 and d^1 molecular complexes we have, in fact, investigated in detail the molecular $[Ti(H_2{}^{17}O)_6]^{3+}$ esaquo complex,[62] which is a typical example of the non-delocalized system. Remarkably we observed in this case a ^{17}O Fermi contact term of the same order (≈8 MHz) which strongly suggests that excess electrons in the blue rutile sample are (at 4 K) largely localized over a single Ti ion, which bears strong similarities to a genuine Ti^{3+} molecular cation.

A totally different scenario is present in the case of anatase (Fig. 9b). No traces of ^{17}O correlation peaks could be found in the (−,+) quadrant of HYSCORE spectra. The only signal observed was a peak centered at the ^{17}O nuclear Larmor frequency, in the (+,+) quadrant with a maximum extension of about 2 MHz. This clearly indicates the sole presence of weakly coupled ^{17}O.

The absence of a distinct ^{17}O coupling in the case of trapping electron centers in anatase is therefore strongly symptomatic of an unpaired electron wave function sampling a larger number of oxide anions and thus indicating the delocalized nature of the defect with drop of the hyperfine interaction to values under the detection limit of the HYSCORE technique. There are three other important elements, besides the described observation, which suggest that a certain degree of delocalization of the Ti^{3+} wavefunction in anatase is the correct physical description for this system. These elements can be discussed as follows:

A delocalized solution is not excluded by theory. The nature of the electron trapped states in titania has been recently tackled by Di Valentin *et al.*[21] who found two opposite solutions (excess electron fully localized in a d_{xy} orbital and electron delocalized over all the d_{xy} orbitals of the supercell used for the calculations) having the same total energy. In the former case Ti^{3+} is an intra band gap state about 0.8 eV (*ca.* 1550 nm, NIR region) below the bottom of the conduction band while the delocalized state lies at the bottom of the conduction band itself. By the way in our optical investigation of n-type doped anatase (Nb or F doped) we never found evidence of NIR absorption.

The nature of signal A must be considered again in the perspective of the electron localisation problem. Signal A (Fig. 2, Table 1) has an axial structure fully confirmed even under the high resolution conditions of EPR recorded in the W band (EPR 90 GHz). The axial nature of the *g* tensor is not compatible with the local symmetry of Ti^{4+} ions in unperturbed bulk anatase (Scheme 3) which shows quite strong distortions in the equatorial plane and the absence of fourfold (or threefold)

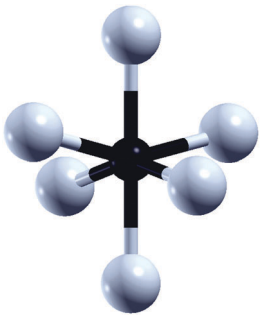

Scheme 3 The local symmetry of Ti ions in anatase.

axes required to ensure the axial symmetry of *g*. In other words, a hypothetical molecular compound of Ti^{3+} with the symmetry shown in Scheme 3 could not have an axial *g* tensor. One could infer that the localization of an extra-electron most likely induces polarisation of the original trapping site, however an increase of its symmetry upon trapping, leading to an axial situation, seems rather unlikely. It is not surprising in fact that in the case of rutile electron trapping in sites having geometry quite similar to that shown for anatase generates in all cases rhombic signals (Table 1, signals C and D). The nature of signal A therefore, in agreement with HYSCORE results, most probably corresponds to an electron delocalization over a discrete number of lattice sites with a wavefunction maintaining the typical axial symmetry clearly indicated by the *g* tensor.

The different behaviour of anatase and rutile in terms of electron conduction properties is known from the literature. By a careful comparison of conductivities and the Hall effect of rutile and anatase single crystal films annealed under vacuum at 673 K and 723 K, H. Tang *et al.*[63] individuated a marked difference in the behavior of the two polymorphs. The reduced rutile resistivity decreases with decreasing temperature and conduction is ensured either by thermal excitation in the CB (at high temperature) or by hopping from donor (Ti^{3+}) centers. The donor state radius is evaluated, in this case, of the order of 2.6 Å. Conductivity of partially reduced anatase is of metallic type and nearly constant with temperature. Under such conditions, and differently from rutile, the Hubbard gap in the donor bands vanishes. The effective mass of the carrier is small and the Bohr radius of the donor state is around 15 Å significantly exceeding the interionic distance. A further element of difference is given by the position, in the two cases, of the energy levels of excess electron centres (Ti^{3+}). In the case of rutile (interstitial sites, coloured material) these ions correspond to localized states well below the conduction band. In the case of anatase, when the

only signal A is present (Fig. 2a), the material does not show absorption in the visible range (see point a in this section) and the Ti^{3+} should resonate with the conduction band, in agreement with the proposed model of electron delocalisation.

These data establish a clear-cut separation of the behavior of anatase and rutile and seem in agreement with our data on electron localization in the two polymorphs.

6. Conclusions

In the present paper we have attempted to rationalize, using the Electron Paramagnetic Resonance approach, the problem of electron trapping in titanium dioxide polymorphs individuating, without ambiguity, the EPR signals corresponding to well defined trap sites in both anatase and rutile. The signals are characterised in terms of *g* tensor values only because of the lack of magnetic nuclei producing hyperfine structures. The electron trapping Ti^{3+} centers have been obtained using different procedures (photoexcitation, valence induction, surface reactivity and, as often done in surface science studies, thermal annealing *in vacuo*). At variance with that generally thought, a series of independent and well defined EPR signals can be found in all cases examined with the only exception of the surface Ti^{3+} centres in anatase which, though being characterised by a definite *g* value at 1.93, display a very broad and substantially featureless signal due to site heterogeneity. In the other cases (regular lattice centers in bulk anatase and in rutile, interstitial centers in rutile) we have provided (Table 2) guidelines to individuate the features of each centre. As to the interstitial form of Ti^{3+} in rutile it has been shown that it forms in particularly non-stoichiometric reduced systems (blue rutile) while softer reducing methods tend to cause electron trapping in regular lattice sites (bulk or surface). The question of the degree of localisation of the electrons in the trap is at the centre of a lively debate. In a recent paper by Krüger *et al.*, performed using Resonant Photoelectron Diffraction[32] the question was raised in these terms: *''There is however no experimental answer to the question on which Ti sites the excess electrons are localized and this is because there has been, to date, no suggestion of any relevant experimental approach to unravel charge localization.''* We have contributed to the debate using an experimental approach based on hyperfine EPR techniques (namely HYSCORE) coupled to ^{17}O isotopic substitution obtained *via* specific synthesis. In this way we have evidenced a net difference in the two cases which was possible to explore (interstitial rutile and bulk anatase). In the former case (Table 3) the spin density on the six oxygens surrounding the Ti centre is typical of a true molecular cation with the unpaired electron largely localized over a single Ti ion. In contrast, in the case of anatase lattice centres the spin density on the oxygen ions is much lower suggesting a high degree of delocalisation of the excess electron wave function. These findings, which could find further and conclusive confirmation if materials enriched with ^{47}Ti and ^{49}Ti isotopes would be available, represent a contribution to the scientific debate on titanium dioxide and in particular on some unresolved problems such as that concerning the different photochemical and photocatalytic properties of the two main polymorphs.

Acknowledgements

This work has been supported by the Italian Ministry of University and Research, MIUR through the funds ''Programs of National Relevance'' (PRIN-2009) and the ''National Funding for Basic Research'' with a project entitled ''Oxides at the nanoscale: functionalities and applications'' (FIRB 2011, RBAP115AYN). We also wish to acknowledge the support of the COST Action CM1104, ''Reducible oxides, chemistry, structure and functions''.

References

1 K. Honda and A. Fujishima, *Nature*, 1972, **238**, 37.
2 A. L. Linsebigler, G. Q. Lu and J. T. Yates, *Chem. Rev.*, 1995, **95**, 735.
3 A. Fujishima, T. N. Rao and D. A. Tryk, *J. Photochem. Photobiol., C*, 2000, **1**, 1.
4 *Photocatalysis: Fundamentals and Applications*, ed. N. Serpone and E. Pelizzetti, Wiley & Sons, Chichester, 1989.
5 A. Fujishima, X. Zhang and D. A. Tryk, *Surf. Sci. Rep.*, 2008, **63**, 515.
6 M. Cho, H. Chung, W. Choi and J. Yoon, *Water Res.*, 2004, **38**, 1069.
7 M. Nozawa, K. Tanigawa, M. Hosomi, T. Chikusa and E. Kawada, *Water Sci. Technol.*, 2001, **44**, 127.
8 T. Watanabe, A. Nakajima, R. Wang, M. Minabe, S. Koizumi, A. Fujishima and K. Hashimoto, *Thin Solid Films*, 1999, **351**, 260.
9 A. Hagfelt and M. Grätzel, *Chem. Rev.*, 1995, **95**, 49.
10 X. Chen and S. S. Mao, *Chem. Rev.*, 2007, **107**, 288.
11 M. Chiesa, C. Paganini and E. Giamello, *Appl. Magn. Reson.*, 2010, **37**, 605.
12 U. Diebold, *Surf. Sci. Rep.*, 2003, **48**, 53–229.
13 T. L. Thompson and J. T. Yates, *Chem. Rev.*, 2006, **106**, 442.
14 M. A. Henderson, *Surf. Sci. Rep.*, 2011, **66**, 18.
15 P. W. Tasker, *J. Phys. C: Solid State Phys.*, 1979, **12**, 4977.
16 J. P. La Femina, *Crit. Rev. Surf. Chem.*, 1994, **3**, 297.
17 (*a*) N. A. Deskins and M. Dupuis, *J. Phys. Chem. C*, 2009, **113**, 346–358; (*b*) N. A. Deskins, R. Rousseau and M. Dupuis, *J. Phys. Chem. C*, 2010, **114**, 5891.
18 (*a*) Z. Lin, A. Orlov, R. M. Lambert and M. C. Payne, *J. Phys. Chem. B*, 2005, **109**, 20948; (*b*) C. Di Valentin, G. Pacchioni and A. Selloni, *Phys. Rev. Lett.*, 2006, **97**, 166803; (*c*) E. Finazzi, C. Di Valentin and G. Pacchioni, *J. Phys. Chem. C*, 2009, **113**, 3382; (*d*) S. Cretién and H. Metiu, *J. Phys. Chem. C*, 2011, **115**, 4696.
19 G. Li, N. Dimitrijevic, L. Chen, G. Nichols, T. Rajh and K. A. Gray, *J. Am. Chem. Soc.*, 2008, **130**, 5402.
20 V. N. Kuznetsov and N. Serpone, *J. Phys. Chem. C*, 2009, **113**, 15110.
21 C. Di Valentin, G. Pacchioni and A. Selloni, *J. Phys. Chem. C*, 2009, **113**, 20543.

22 M. A. Henderson, W. S. Epling, C. H. F. Peden and C. L. Perkins, *J. Phys. Chem. B*, 2003, **107**, 534.
23 V. M. Komenko, K. Langer, H. Rager and A. Fett, *Phys. Chem. Miner.*, 1998, **25**, 338.
24 R. L. Kurtz, R. Stock-Bauer and T. E. Madey, *Surf. Sci.*, 1989, **218**, 178.
25 (*a*) R. D. Iyengar, M. Codell, J. S. Karra and J. Turkevich, *J. Am. Chem. Soc.*, 1966, **88**, 5055; (*b*) P. Meriaudau, M. Che and C. K. Jørgensen, *Chem. Phys. Lett.*, 1970, **5**, 1313; (*c*) M. Aono and R. R. Hasiguti, *Phys. Rev. B: Condens. Matter Mater. Phys.*, 1993, **48**, 12406; (*d*) O. I. Micic, Y. N. Zhang, K. R. Cromack, A. D. Trifunac and M. C. Thurnauer, *J. Phys. Chem. B*, 1993, **97**, 7277; (*e*) J. M. Coronado, A. J. Maira, J. C. Conesa, K. L. Yeung, V. Augugliaro and J. Soria, *Langmuir*, 2001, **17**, 5368; (*f*) M. Li, W. Hebenstreit, U. Diebold, A. M. Tyryshkin, M. K. Bowman, G. G. Dunham and M. A. Henderson, *J. Phys. Chem. B*, 2000, **104**, 4944; (*g*) A. L. Attwood, D. M. Murphy, J. L. Edwards, T. A. Egerton and R. W. Harrison, *Res. Chem. Intermed.*, 2003, **29**, 449; (*h*) T. Berger, M. Sterrer, O. Diwald and E. Knozinger, *J. Phys. Chem. B*, 2005, **109**, 6061; (*i*) D. C. Hurum and K. A. Gray, *J. Phys. Chem. B*, 2005, **109**, 977.
26 M. Chiesa and E. Giamello, in *Electron Paramagetic Resonance of Charge Carriers in Solids*, ed. M. Brustolon and E. Giamello, Electron Paramagnetic Resonance: a practitioner's toolkit, Wiley, 2010.
27 M. Chiesa, E. Giamello and M. Che, *Chem. Rev.*, 2010, **110**, 1320.
28 P. H. Zimmerman, *Phys. Rev. B: Condens. Matter Mater. Phys.*, 1973, **8**, 3917.
29 S. Yang, L. E. Halliburton, A. Manivannan, P. H. Bunton, D. B. Baker, M. Kemm, S. Horn and A. Fujishima, *Appl. Phys. Lett.*, 2009, **94**, 162114.
30 S. Yang and L. E. Halliburton, *Phys. Rev. B: Condens. Matter Mater. Phys.*, 2010, **81**, 035204.
31 (*a*) R. Howe and M. Gratzel, *J. Phys. Chem.*, 1985, **89**, 4495; (*b*) R. F. Howe and M. Gratzel, *J. Phys. Chem.*, 1987, **91**, 3906.
32 P. Krüger, S. Bourgeois, B. Domenichini, H. Magnan, D. Chandesris, P. Le Fevre, A. M. Flank, J. Jupille, L. Floreano, A. Cossaro, A. Verdini and A. Morgante, *Phys. Rev. Lett.*, 2008, **100**, 055501.
33 S. Wendt, P. T. Sprunger, E. Lira, G. K. H. M. Madsen, Z. Li, J. Hansen, J. Matthiensen, A. Blekinge-Rasmussen, E. Laegsgaard, B. Hammer and F. Besenbacher, *Science*, 2008, **320**, 1755.
34 (*a*) C. Di Valentin, G. Pacchioni, A. Selloni, S. Livraghi and E. Giamello, *J. Phys. Chem. B*, 2005, **109**, 11414; (*b*) S. Livraghi, M. C. Paganini, E. Giamello, A. Selloni, C. Di Valentin and G. Pacchioni, *J. Am. Chem. Soc.*, 2006, **128**, 15666; (*c*) S. Livraghi, M. R. Chierotti, E. Giamello, G. Magnacca, M. C. Paganini, G. Cappelletti and C. L. Bianchi, *J. Phys. Chem. C*, 2008, **112**, 17244; (*d*) F. Napoli, M. Chiesa, S. Livraghi, E. Giamello, S. Agnoli, G. Granozzi, G. Pacchioni and C. Di Valentin, *Chem. Phys. Lett.*, 2009, **477**, 135; (*e*) G. Barolo, S. Livraghi, M. Chiesa, M. C. Paganini and E. Giamello, *J. Phys. Chem. C*, 2012, **116**, 20887.
35 *Electron Paramagnetic Resonance. A Practitioner's toolkit*, ed. M. Brustolon and E. Giamello, Wiley, Hoboken (USA), 2009.
36 P. Pietrzyk, Z. Sojka and E. Giamello, in *Electron Paramagnetic Resonance Spectroscopy*, ed. M. Che and J. Vedrine, Characterisation of Solid Materials and Heterogeneous Catalysts, Wiley VCH Verlag GmbH & Co. KGaA, 2012, pp. 343–406.
37 M. Chiesa, E. Giamello, C. Di Valentin and G. Pacchioni, *Chem. Phys. Lett.*, 2005, **403**, 124.
38 J. Kiwi, J. T. Suss and S. Zsapiro, *Chem. Phys. Lett.*, 1984, **106**, 135.
39 M. Valigi, D. Cordischi, G. Minelli, P. Natale, P. Porta and C. P. Kreijzers, *J. Solid State Chem.*, 1988, **77**, 255.
40 S. Yang and L. E. Halliburton, *Phys. Rev. B: Condens. Matter Mater. Phys.*, 2010, **81**, 035204.
41 A. M. Czoska, S. Livraghi, M. Chiesa, E. Giamello, E. Finazzi, C. Di Valentin, G. Pacchioni, S. Agnoli and G. Granozzi, *J. Phys. Chem. C*, 2008, **112**, 8951.
42 S. Livraghi, M. Chiesa, M. C. Paganini and E. Giamello, *J. Phys. Chem. C*, 2011, **115**, 25413.
43 O. Micic, Y. Zhang, C. Cromack, A. Trifunac and M. Thurnauer, *J. Phys. Chem.*, 1993, **97**, 1211.
44 (*a*) D. C. Hurum, A. G. Agrios, K. A. Gray, T. Rajh and M. Thurnauer, *J. Phys. Chem. B*, 2003, **107**, 4545; (*b*) D. C. Hurum, K. A. Gray, T. Rajh and M. Thurnauer, *J. Phys. Chem. B*, 2005, **109**, 977; (*c*) D. C. Hurum, A. G. Agrios, S. E. Crist, K. A. Gray, T. Rajh and M. Thurnauer, *J. Electron Spectrosc. Relat. Phenom.*, 2006, **150**, 155.
45 P. F. Chester, *J. Appl. Phys.*, 1961, **32**, 866.
46 P. H. Zimmerman, *Phys. Rev. B: Condens. Matter Mater. Phys.*, 1973, **8**, 3917.
47 D. L. Griscom, *Phys Rev. B: Condens. Matter Mater. Phys.*, 1989, **40**, 4224.
48 C. Gionco, M. C. Paganini, E. Giamello, unpublished work.
49 M. Chiesa, M. C. Paganini, E. Giamello, D. M. Murphy, C. Di Valentin and G. Pacchioni, *Acc. Chem. Res.*, 2006, **39**, 861.
50 T. Berger, O. Diwald, E. Knoezinger, F. Napoli, M. Chiesa and E. Giamello, *Chem. Phys.*, 2007, **339**, 138.
51 T. Rajh, A. E. Ostafin, O. I. Micic, D. M. Tiede and M. C. Thurnauer, *J. Phys. Chem.*, 1996, **100**, 4538.
52 (*a*) M. A. Henderson, *Surf. Sci.*, 1995, **343**, L1156–L1160; (*b*) M. A. Henderson, *Surf. Sci.*, 1999, **419**, 174.
53 M. Li, W. Hebenstreit, U. Diebold, A. M. Tyryshkin, M. K. Bowman, G. G. Dunham and M. A. Henderson, *J. Phys. Chem. B*, 2000, **104**, 4944.
54 M. Aono and R. R. Hasiguti, *Phys. Rev. B: Condens. Matter Mater. Phys.*, 1993, **48**, 12406.
55 M. Xing, W. Fang, M. Nasir, Y. Maa, J. Zhang and M. Anpo, *J. Catal.*, 2013, 297–236; F. Zuo, L. Wang, T. Wu, Z. Zhang, D. Borchardt and P. Feng, *J. Am. Chem. Soc.*, 2010, **132**, 11856; T. R. Gordon, M. Cargnello, T. Paik, F. Mangolini, T. Weber, P. Fornasiero and C. B. Murray, *J. Am. Chem. Soc.*, 2012, **134**, 6751.

56 S. Livraghi, S. Maurelli, M. C. Paganini, M. Chiesa and E. Giamello, *Angew. Chem., Int. Ed.*, 2011, **50**, 8038.
57 S. D. Eliot and S. P. Bates, *Phys. Chem. Chem. Phys.*, 2001, **3**, 1954.
58 E. Finazzi, C. Di Valentin and G. Pacchioni, *J. Phys. Chem. C*, 2009, **113**, 3382.
59 (*a*) M. Chiesa, P. Martino, E. Giamello, C. Di Valentin and G. Pacchioni, *J. Phys. Chem. B*, 2004, **108**, 11529; (*b*) M. Chiesa, E. Giamello, C. Di Valentin, G. Pacchioni, Z. Sojka and S. Van Doorslaer, *J. Am. Chem. Soc.*, 2005, **127**, 16935; (*c*) M. Chiesa, M. C. Paganini, E. Giamello, C. Di Valentin and G. Pacchioni, *ChemPhysChem*, 2006, **7**, 728.
60 J. K. Burdett, *Inorg. Chem.*, 1985, **24**, 2244.
61 D. Baute and D. Goldfarb, *J. Phys. Chem. A*, 2005, **109**, 7865.
62 S. Maurelli, S. Livraghi, M. Chiesa, E. Giamello, S. Van Doorslaer, C. Di Valentin and G. Pacchioni, *Inorg. Chem.*, 2011, **50**, 2385.
63 H. Tang, K. Prasad, R. Sanjines, P. E. Schmid and F. Lévy, *J. Appl. Phys.*, 1994, **75**, 2042.